NASA Contractor Report 201710

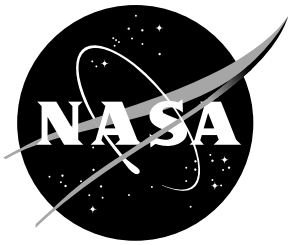

Analysis of Waveguide Junction Discontinuities Using Finite Element Method

Manohar D. Deshpande
ViGYAN, Inc., Hampton, Virginia

Contract NAS1-19341

July 1997

National Aeronautics and
Space Administration
Langley Research Center
Hampton, Virginia 23681-0001

Contents

List of Figures

List of Symbols

a_0	dominant mode reflection coefficient
a_p	complex waveguide modal amplitude of p^{th} mode in region I
b_m	complex amplitude associated with tetrahedral basis function
[b]	column matrix
b_0	dominant mode amplitude in region III
b_p	complex waveguide modal amplitude of p^{th} mode in region III
$\vec{E}\big\|_{over\ S_1}$	tangential electric field vector over the plane P_1
$\vec{E}\big\|_{over\ S_2}$	tangential electric field vector over the plane P_2
$\vec{E}^{I}(x, y, z)$	transverse electric field vector in region I
$\vec{E}^{II}(x, y, z)$	electric field vector in region II
$\vec{E}^{III}(x, y, z)$	transverse electric field vector in region III
$\overrightarrow{e_{10}}$	dominant vector modal function for region I
$\overrightarrow{e_{1p}}$	rectangular waveguide vector modal function for pth mode for region I
$\overrightarrow{e_{20}}$	dominant vector modal function for region III
$\overrightarrow{e_{2p}}$	rectangular waveguide vector modal function for pth mode for region III
$\vec{H}^{I}(x, y, z)$	transverse magnetic field vector in region I
$\vec{H}^{II}(x, y, z)$	magnetic field vector in region II
$\vec{H}^{III}(x, y, z)$	transverse magnetic field vector in region III
$\overrightarrow{h_{10}}$	dominant vector modal function for region I
$\vec{h}_{1p}$	rectangular waveguide vector modal function for p^{th} mode for region I
$\vec{h}_{2p}$	rectangular waveguide vector modal function for p^{th} mode for region I
j	$\sqrt{-1}$
k_0	free-space wave number
$[S]$	global finite element matrix
$[S_{el}]$	element matrix for single tetrahedral element

S_1	surface area over plane P_1
S_2	surface area over plane P_2
S_{11}	return loss in dominant mode at plane P_1
S_{21}	transmission coefficient in dB at plane P_2
$\vec{T}(x, y, z)$	vector testing function
TE_{10}	dominant mode
$[v]$	excitation column vector
W_{x1}, W_{x2}	x-dimensions of rectangular waveguide
W_y	y-dimension of rectangular waveguide
$\overrightarrow{W_m}$	vector basis function associated with tetrahedron
x, y, z	Cartesian Coordinate system
Y_{10}	dominant modal admittance for region I
Y_{1p}	modal admittance of p^{th} mode for region I
Y_{2p}	modal admittance of p^{th} mode for region III
ε_0	permittivity of free-space
μ_0	permeability of free-space
ε_r	relative permittivity of medium in region II
μ_r	relative permeability of medium in region II
γ_{10}	dominant mode propagation constant for region I
γ_{1p}	propagation constant for p^{th} mode for region I
γ_{2p}	propagation constant for p^{th} mode for region III
ω	angular frequency

Abstract

A Finite Element Method (FEM) is presented to determine reflection and transmission coefficients of rectangular waveguide junction discontinuities. An H-plane discontinuity, an E-plane ridge discontinuity and a step discontinuity in a concentric rectangular waveguide junction are analyzed using the FEM procedure. Also, reflection and transmission coefficients due to presence of a gap between two sections of a rectangular waveguide are determined using the FEM. The numerical results obtained by the present method are in excellent agreement with the earlier published results. The numerical results obtained by the FEM are compared with the numerical results obtained using Mode Matching Method (MMM) and also with the measured data.

1.0 Introduction

A slotted rectangular waveguide array antenna is being proposed to be used in a microwave scattrometer for soil moisture measurements. During the launch phase of such a scatterometer, the slotted waveguide should be folded. After full deployment of the scatterometer, the waveguide must be unfolded to its full length. Due to the mechanical imperfection of the joints and hinges, there will be misalignments and gaps. These gaps and misalignments will affect the performance of the slot array. It is the purpose of this report to analyze the effects of the gaps and misalignments on the transmission line properties of rectangular waveguide sections. However, the effect of these gaps and misaligmnents on the performance of the slot array will not be considered here.

The types of misalignments and gaps that may occur after unfolding the various sections of rectangular waveguide are shown in figure 1

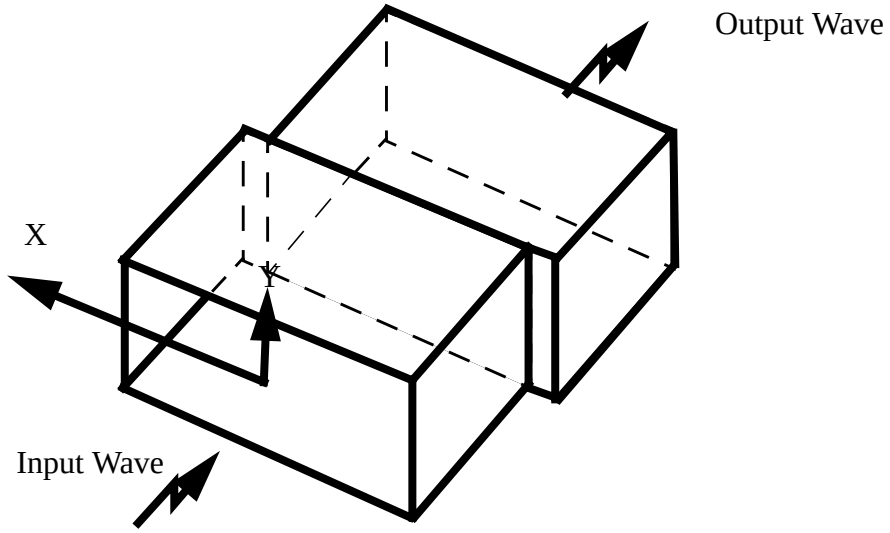

Figure 1(a) Rectangular waveguide with misalignment in x-direction.
(Waveguide flanges are not shown)

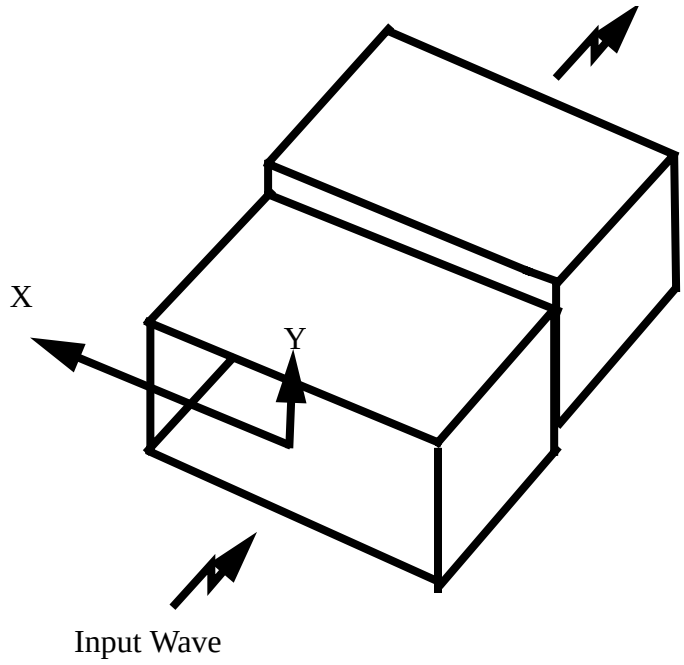

Figure1(b) Rectangular waveguide junction with misalignment in y-dimension.

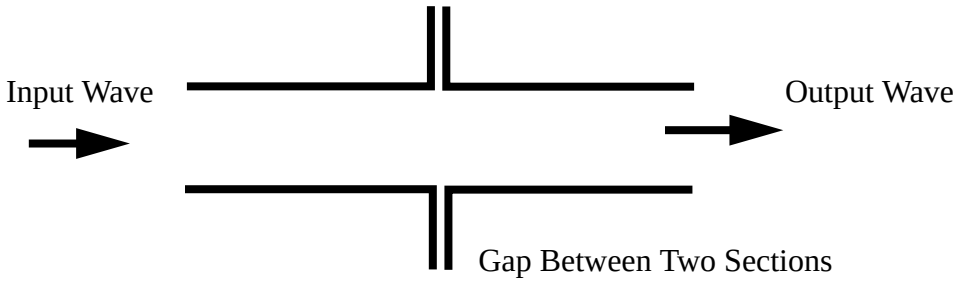

Figure 1(c) Rectangular waveguide junction with a gap.

For assessment of the effects of such discontinuities on the transmission and reflection properties of rectangular waveguide, many analytical techniques can be used. The modelling of waveguide junction discontinuities has been a subject that has been studied considerably in the past. An equivalent circuit approach based on an electrostatic approximation and variational principle [1-4] has been used to analyze these discontinuities. However, these approximate techniques may not be accurate for electrically large discontinuities. Furthermore, only single mode interactions are accounted in these simple representations . Higher order mode interactions are taken into account by using the mode matching technique[5,6]. In the MMM, the fields in each region across the junction are expressed in terms of infinite number of waveguide modal functions. Application of continuity of tangential components of electric and magnetic fields across the junction in conjunction with the Method of Moments (MoM) yields a matrix equation with tangential fields over the junction as an unknown variable. From the solution of the matrix

equation, the reflection and transmission properties of the waveguide junction are determined. The resulting code, although accurate, can be computationally inefficient. There are different versions of the MMM reported in the literature such as generalized scattering matrix (GSM) [7] techniques, multimodal network representation methods using admittance, or impedance matrix representation [8-10]. The MMM is mostly applied to analyze zero-thickness discontinuities at the junctions. For non-zero thickness discontinuties in the direction of propagation, the mode matching techniques become quite involved. Furthermore, it is cumbersome to apply the MMM when the waveguide junctions are loaded with three-dimensional arbitrarily-shaped discontinuities. In such cases, a numerical technique such as the FEM [11-13] is more versatile and easily adaptable to changes in the structures of discontinuities. In this report, a numerical technique using the FEM is developed to analyze step discontinuities as well as three-dimensional arbitrarily-shaped discontinuities present at the rectangular waveguide junctions.

In [11], reflection and transmission characteristics of metal wedges in a rectangular waveguide were studied using H-field FEM formulation. It has been shown in [11] that the vector edge based formulation eliminates the spurious solutions. In this report, the FEM using the E-field formulation is developed to analyze rectangular waveguide junction discontinuities. Because of the metal boundaries of rectangular waveguide, the E-formulation results in fewer unknowns compared with the H-field formulation of [11].

The remainder of this report is organized as follows. The FEM formulation of the waveguide junction problem using the weak form of the Helmoltz wave equation is developed in section 2. Also in section 2, MMM formulation is presented to determine reflection and transmission coefficients of transverse discontinuities in a rectangular waveguide. Numerical results on the transmission and reflection coefficients for E-plane and H-plane step

discontinuities are given in section 3 along with earlier published results for comparison. Also in section 3, the experimental results on some of the waveguide junction discontinuities measured in the Material Measurement Laboratory of the Electromagnetics Research Branch are compared with the results obatined using the present approach. The report concludes in section 4 with remarks on advantages and limitations of the present technique.

2.0 Theory

2.1 Finite Element Formulation:

In this section, the FEM will be used to determine the reflection and transmission coefficients of the rectangular waveguide junction discontinuity shown in Figure 2.

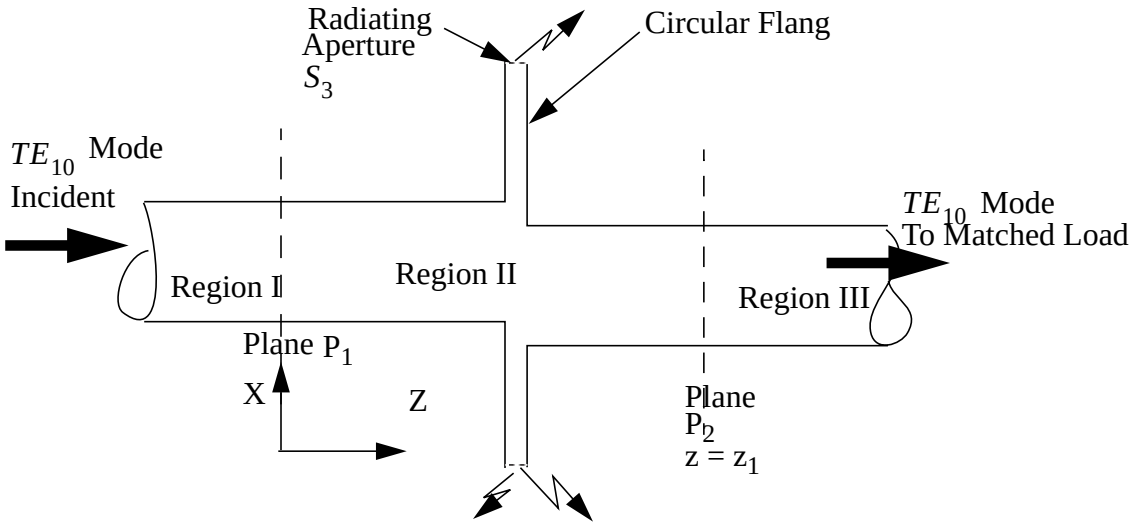

Figure 2 Geometry of rectangular waveguide junction with step discontinuity and gap.

It is assumed that the waveguide is excited by a dominant TE_{10} mode from the left. To analyze the junction discontinuity, the junction is assumed to be enclosed by two planes: P_1 and P_2. The planes P_1 and P_2 divide the waveguide region into three regions as shown in Figure 2. The air gap at the junction between two waveguide sections causes leakage of electromag-

netic energy which is accounted in the present formulation. Using the waveguide vector modal functions, the transverse electromagnetic field in region I is expressed as [16]

$$\vec{E}^{I}(x,y,z) = \hat{e}_{10}(x,y)\, e^{-j\gamma_{10} z} + \sum_{p=0}^{\infty} a_p \hat{e}_{1p}(x,y)\, e^{j\gamma_{1p} z} \tag{1}$$

$$\vec{H}^{I}(x,y,z) = \hat{h}_{10}(x,y)\, Y_{10}\, e^{-j\gamma_{10} z} - \sum_{p=0}^{\infty} a_p \hat{h}_{1p}(x,y)\, Y_{1p}\, e^{j\gamma_{1p} z} \tag{2}$$

In deriving equations (1) and (2), it is assumed that only the dominant mode is incident on the interface P_1 and the a_p is the amplitude of reflected modes at the z=0 plane. Y_{1p} and γ_{1p} appearing in equations (1) and (2) are respectively the characteristic admittance and propagation constant for p^{th} mode and are defined in [16]. The unknown complex modal amplitude a_p may be obtained in terms of the transverse electric field over the plane P_1 as follows

$$1 + a_0 = \iint_{S_1} \vec{E}\Big|_{over\ P_1} \bullet \hat{e}_{10}\, ds \tag{3}$$

$$a_p = \iint_{S_1} \vec{E}\Big|_{over\ P_1} \bullet \hat{e}_{1p}\, ds \tag{4}$$

where S_1 is the surface area over the plane P_1.

Likewise, the transverse components of electric and magnetic fields in the region III can be written as [16]

$$\vec{E}^{III}(x,y,z) = \sum_{p=0}^{\infty} b_p \vec{e}_{2p}(x,y) e^{j\gamma_{2p} z} \tag{5}$$

$$\vec{H}^{III}(x,y,z) = \sum_{p=0}^{\infty} b_p \vec{h}_{2p}(x,y)\, Y_{2p}\, e^{j\gamma_{2p} z} \tag{6}$$

where b_p is the amplitude of transmitted mode at the $z=z_2$ plane, Y_{2p} and γ_{2p} appearing in equations (5) and (6) are respectively the characteristic admittance and propagation constant for p^{th} mode for output waveguide and are defined in [16]. The unknown complex modal amplitude b_p may be obtained in terms of the transverse electric field over the plane P_2 as follows

$$b_p = \int\int_{S_2} \vec{E}\Big|_{over\ P_2} \bullet \vec{e}_{2p} ds$$

where S_2 is the surface area over the plane P_2.

The electromagnetic field inside region II is obtained using the FEM formulation [17]. The vector wave equation for the $\vec{E}^{II}$ field is given by

$$\nabla\times\left(\frac{1}{\mu_r}\cdot\nabla\times\vec{E}^{II}\right)-\left(k_0^2\varepsilon_r\right)\vec{E}^{II} = 0 \tag{7}$$

Using the weak form of the vector wave equation and some mathematical manipulation [17], the equation (5) may be written as

$$\iiint_V\left(\nabla\times\vec{T}\bullet\left(\frac{1}{\mu_r}\nabla\times\vec{E}^{II}\right)-\left(k_0^2\varepsilon_r\right)\vec{E}^{II}\bullet\vec{T}\right)dv = 2j\omega\mu_0\, Y_0 \int\int_{S_1}\vec{T}\bullet\vec{e}_0(x,y)\,ds$$

$$-j\omega\mu_0\sum_{p=0}^{\infty} Y_{1p}\left(\left(\int\int_{S_1}\vec{T}\bullet\vec{e}_{1p}(x,y)\,ds\right)\left(\int\int_{S_1}\vec{E}^{II}\Big|_{over P_1}\bullet\vec{e}_{1p}(x,y)\,ds\right)\right)$$

$$-j\omega\mu_0 \sum_{p=0}^{\infty} Y_{2p} \left(\left(\iint_{S_2} \vec{T} \bullet \vec{e}_{2p}(x,y)\, ds \right) \left(\iint_{S_2} \vec{E}^{II}\Big|_{over P_2} \bullet \vec{e}_{2p}(x,y)\, ds \right) \right)$$

$$-j\omega\mu_0 \iint_{S_3} T \times \hat{n} \bullet \vec{H}_{ap} ds \tag{8}$$

where S_2 is the cross sectional area at plane P_2, S_3 is the surface area of radiating aperture, and $\vec{H}_{ap}$ is the magnetic field in the radiating aperture S_3. In order to solve the equation (9), the volume enclosed by region II is discretized by using first-order tetrahedral elements. The electric field in a single tetrahedron is represented as

$$\vec{E}^{II} = \sum_{m=1}^{6} b_m \cdot \vec{W}_m \tag{9}$$

where b_m are the six complex coefficients of electric field associated with the six edges of the tetrahedron, and $\vec{W}_m(x,y,z)$ is the vector basis function associated with the m^{th} edge of the tetrahedron. A detailed derivation for the expressions for $\vec{W}_m(x,y,z)$ is given in reference [17]. Substituting equation (10) into equation (9), integration over the volume of one tetrahedron results in the element matrix equation

$$\left[S_{el}\right]\left[b\right] = \left[v\right] \tag{10}$$

where the entries in the element matrices are given by

$$S_{el}(m,n) = \frac{1}{\mu_r} \left(\iiint_V \left(\nabla \times \vec{W}_m \bullet \nabla \times \vec{W}_n - k_0^2 \varepsilon_r \vec{W}_n \bullet \vec{W}_m \right) dv \right)$$

$$+ \quad (j\omega\mu_0) \sum_{p=0}^{\infty} Y_{1p} \left(\left(\iint_{S_1} \vec{W}_m \bullet \vec{e}_{1p}(x,y)\, ds \right) \left(\iint_{S_1} \vec{W}_n \bullet \vec{e}_{1p}(x,y)\, ds \right) \right)$$

$$+ \quad (j\omega\mu_0) \sum_{p=0}^{\infty} Y_{2p} \left(\left(\iint_{S_2} \vec{W}_m \bullet \hat{e}_{2p}(x,y)\, ds \right) \left(\iint_{S_2} \vec{W}_n \bullet \hat{e}_{2p}(x,y)\, ds \right) \right)$$

$$(-j\omega\mu_0) k_0^2 \iint_{S_3} \left((\vec{W}_m \times \hat{n}) \bullet \frac{1}{4\pi} \iint_{S_3} \left(\vec{W}_n \times \hat{n} \frac{e^{-jk_0(|\hat{r}-\hat{r}'|)}}{|\hat{r}-\hat{r}'|} ds' \right) \right) ds$$

$$+ \quad j\omega\mu_0 \iint_{S_3} \left(\nabla\bullet(\vec{W}_m \times \hat{n}) \bullet \frac{1}{4\pi} \iint_{S_3} \left(\nabla\bullet(\vec{W}_n \times \hat{n}) \frac{e^{-jk_0(|\hat{r}-\hat{r}'|)}}{|\hat{r}-\hat{r}'|} ds' \right) \right) ds \qquad (11)$$

$$v(m) = 2(j\omega\mu_0)\, Y_{10} \iint_{S_1} \overrightarrow{W_m} \bullet \hat{e}_{10}(x,y)\, ds \qquad (12)$$

These element matrices can be assembled over all the tetrahedral elements in the region II to obtain a global matrix equation

$$[S][b] = [v] \qquad (13)$$

The solution vector $[b]$ of the matrix equation (14) is then used in equation (3) to determine the reflection coefficient at the reference plane P_1 as

$$a_0 = -1 + \iint_{S_1} \vec{E}\big|_{over\ P_1} \bullet \hat{e}_{10} ds \qquad (14)$$

The transmission coefficient at the plane P_2 is obtain as [18]

$$b_0 = \sqrt{\frac{\gamma_{20}}{\gamma_{10}}} \iint_{S_2} \vec{E}\big|_{over\ P_2} \bullet \hat{e}_{20} ds \qquad (15)$$

The return loss and power transmitted through the rectangular junction are then calculated using

$$S_{11} = 20.\log(|a_0|) \qquad (16)$$

$$S_{21} = 20.\log(|b_0|) \qquad (17)$$

The power transmitted through the junction can also be calculated using

$$S_{21} = 20.\log\left(\sqrt{1 - \sum_{p=1}^{P} |a_p|^2} \right) \qquad (18)$$

where the summation should be done over the propagating modes only.

2.2 Mode Matching Method:

In this section the MMM for the rectangular waveguide junction discontinuities is presented. Since the modelling of air gap between the two waveguide sections using the MMM is quite involved, the junction discontinuities of E- and H-plane steps types (as shown in fig. 3) are only considered.

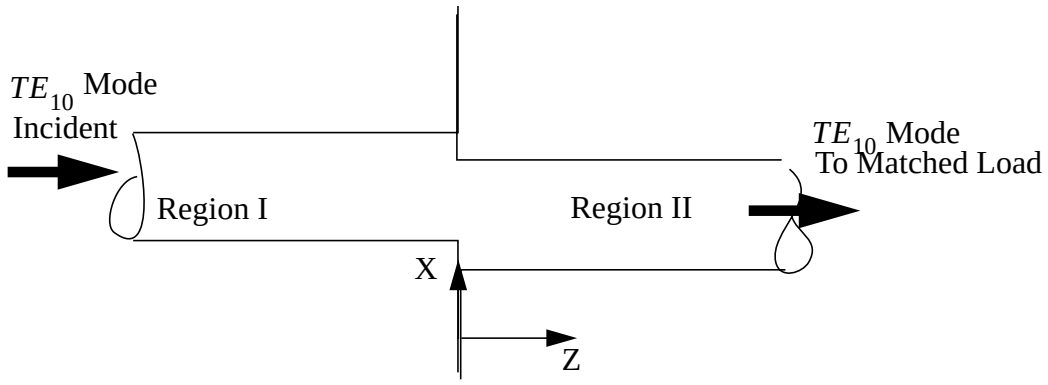

Figure 3 Geometry of waveguide junction discontinuity without an air gap.

The transverse components of electric and magnetic fields in the region I and II can be written as

$$\vec{E}^{I}(x,y,z) = \hat{e}_{10}(x,y)\, e^{-j\gamma_{10} z} + \sum_{p=0}^{\infty} a_p \hat{e}_{1p}(x,y)\, e^{j\gamma_{1p} z} \qquad (19)$$

$$\vec{H}^{I}(x,y,z) = \hat{h}_{10}(x,y)\, Y_{10}\, e^{-j\gamma_{10} z} - \sum_{p=0}^{\infty} a_p \hat{h}_{1p}(x,y)\, Y_{1p}\, e^{j\gamma_{1p} z} \qquad (20)$$

In deriving equations (1) and (2) it is assumed that only the dominant mode is incident from the left and the a_p is the amplitude of reflected modes at the z=0 plane. Y_{1p} and γ_{1p} appearing in equations (1) and (2) are respectively the characteristic admittance and propagation constant for

p^{th} mode and are defined in [16]. The unknown complex modal amplitude a_p may be obtained in terms of the transverse electric field over the z = 0 plane as follows

$$\left(1 + a_0 = \iint_S \vec{\mathrm{E}}\big|_{z=0} \bullet \hat{e}_{10} ds \right) \tag{21}$$

$$a_p = \iint_S \vec{\mathrm{E}}\big|_{z=0} \bullet \hat{e}_{1p} ds \tag{22}$$

where S is the surface area over the z = 0 plane.

Likewise, the transverse components of electric and magnetic fields in the region II can be written as [16]

$$\vec{E}^{II}(x,y,z) = \sum_{p=0}^{\infty} b_p \hat{e}_{2p}(x,y) e^{j\gamma_{2p} z} \tag{23}$$

$$\vec{H}^{II}(x,y,z) = \sum_{p=0}^{\infty} b_p \hat{h}_{2p}(x,y) \; Y_{2p} \, e^{j\gamma_{2p} z} \tag{24}$$

where b_p is the amplitude of transmitted mode at the z=0 plane, Y_{2p} and γ_{2p} appearing in equations (24) and (25) are respectively the characteristic admittance and propagation constant for p^{th} mode for output waveguide and are defined in [16]. The unknown complex modal amplitude b_p may be obtained in terms of the transverse electric field over the z = 0 plane as follows

$$b_p = \iint_S \vec{\mathrm{E}}\big|_{z=0} \bullet \hat{e}_{2p} ds \tag{25}$$

where S is the surface area over the z = 0 plane.

In order to determine the unknown coefficients a_p and b_q we assume the tangential electric field

over the plane z = 0 as

$$\vec{\mathrm{E}}\Big|_{z=0} = \sum_{r=0}^{\infty} c_r \hat{e}_{3r} \tag{26}$$

where c_r is unknown complex coefficient, and $\hat{e}_{3r}$ is the vector mode function for a rectangular waveguide having a cross section same as the cross section of the aperture. Substituting (27) in (22), (23), and (26), the unknown coefficients a_p and b_q are obtained as

$$1 + a_0 = \sum_{r=0}^{\infty} c_r \int\int_{Aperture} \hat{e}_{3r} \bullet \hat{e}_{10} ds \tag{27}$$

$$a_p = \sum_{r=0}^{\infty} c_r \int\int_{Aperture} \hat{e}_{3r} \bullet \hat{e}_{1p} ds \tag{28}$$

$$b_q = \sum_{r=0}^{\infty} c_r \int\int_{Aperture} \hat{e}_{3r} \bullet \hat{e}_{2q} ds \tag{29}$$

Substituting (28)-(30) into (20),(21) and (24),(25), the transverse fields in the regions I and II are obtained as

$$\vec{E}^{I}(\mathrm{x,y,z}) = -2j\hat{e}_{10}(x,y)\sin(\gamma_{10}\,\mathrm{z}) + \sum_{p=0}^{\infty}\left\{\sum_{r=0}^{\infty} c_r \int\int_{Aperture} \hat{e}_{3r} \bullet \hat{e}_{1p} ds\right\}\hat{e}_{1p}(\mathrm{x,y})\, e^{j\gamma_{1p}\mathrm{z}} \tag{30}$$

$$\vec{H}^{I}(\mathrm{x,y,z}) = 2\hat{h}_{10}(x,y)\,\mathrm{Y}_{10}\cos(\gamma_{10}\,\mathrm{z}) - \sum_{p=0}\left\{\sum_{r=0}^{\infty} c_r \int\int_{Aperture} \hat{e}_{3r} \bullet \hat{e}_{1p} ds\right\}\hat{h}_{1p}(\mathrm{x,y})\;\mathrm{Y}_{1p}\, e^{j\gamma_{1p}\mathrm{z}} \tag{31}$$

for the region I and

$$\vec{E}^{II}(x,y,z) = \sum_{q=0}^{\infty} \left\{ \sum_{r=0}^{\infty} c_r \int\int_{Aperture} \vec{e}_{3r} \bullet \vec{e}_{2q} ds \right\} \vec{e}_{2q}(x,y)\, e^{j\gamma_{1q} z} \tag{32}$$

$$\vec{H}^{II}(x,y,z) = \left(\sum_{q=0} \left\{ \sum_{r=0}^{\infty} c_r \int\int_{Aperture} \vec{e}_{3r} \bullet \vec{e}_{2q} ds \right\} \vec{h}_{2q}(x,y) \quad Y_{2q}\, e^{j\gamma_{2q} z} \right) \tag{33}$$

Equating the tangential magnetic fields across the aperture yields an integral equation with c_r unknowns as

$$2\vec{h}_{10}(x,y)\ Y_{10} = \sum_{r=0} c_r \left\{ \sum_{p=0}^{\infty} \int\int_{Aperture} \vec{e}_{3r} \bullet \vec{e}_{1p} ds \right\} \vec{h}_{1p}(x,y) \quad Y_{1p}$$

$$+ \sum_{r=0} c_r \left\{ \sum_{q=0}^{\infty} \int\int_{Aperture} \vec{e}_{3r} \bullet \vec{e}_{2q} ds \right\} \vec{h}_{2q}(x,y) \quad Y_{2q} \tag{34}$$

Taking cross product of (35) with $\hat{z}$ and selecting $\vec{e}_{3r'}$ as a testing function, the integral equation in (35) yields the following set of simultaneous equations

$$2\int\int_{Aperture} \vec{e}_{3r'} \bullet \vec{e}_{10} ds\ Y_{10} = \sum_{r=0} c_r \sum_{p=0}^{\infty} \int\int_{Aperture} \vec{e}_{3r} \bullet \vec{e}_{1p} ds \int\int_{Aperture} \vec{e}_{3r'} \bullet \vec{e}_{1p} ds \quad Y_{1p}$$

$$\sum_{r=0} c_r \sum_{q=0}^{\infty} \int\int_{Aperture} \vec{e}_{3r} \bullet \vec{e}_{2q} ds \int\int_{Aperture} \vec{e}_{3r'} \bullet \vec{e}_{2q} ds \quad Y_{2q} \tag{35}$$

where $r' = 1, 2, 3. \ldots$ By terminating the infinite summations with respect to p to N_p, q to N_q, and r to N_r equation (36) can be solved for c_r. The reflection and transmission coefficients are then obtained as

$$S_{11} = -1 + \sum_{r=0}^{N_r} c_r \int\int_{Aperture} \vec{e}_{3r} \bullet \vec{e}_{10} ds \tag{36}$$

$$S_{21} = \sum_{r=0}^{N_r} c_r \int\int_{Aperture} \hat{e}_{3r} \bullet \hat{e}_{20} ds \qquad (37)$$

3.0 Numerical Results

To validate the present technique, we first present numerical results on the reflection and transmission coefficients for H-plane discontinuity in a x-band rectangular waveguide as shown in Figure 3. This geometry has been solved by earlier researchers using the MMM and CAD-oriented equivalent circuit modelling[19].

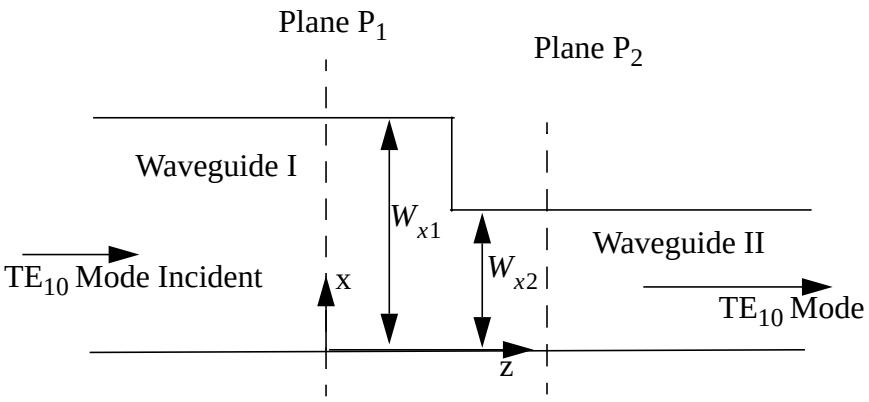

Figure 3 Top view of an H-plane discontinuity in a rectangular waveguide. Waveguide I (W_{x1} = 2.286 cm, W_y = 1.02cm), Waveguide II (W_{x2} = 1.5 cm, W_y = 1.02 cm)

For the present analysis, the plane P_1 was selected at z = 0 and the plane P_2 was selected at z = 1 cm. The junction was at z = 0.5 cm. The reflection and transmission coefficients calculated using the present approach are shown in Figure 4 along with the results obatined by the MMM [19]. There is an excellent agreement between the results of two methods. The transmission curve shown as a dotted line is calculated by $S_{12} = 20\log_{10}\sqrt{(1 - \text{Reflected Power})}$. Seven hundred twenty eight tetrahedral were used to discretize the FEM region.

For further validation of the code, an E-plane ridge waveguide discontinuity in a rectangular waveguide, as shown in Figure 5, is considered. The transmission coefficient in the presence of the metallic ridge is calculated using the present code as a function of frequency and is presented in Figure 6 along with the earlier published data. There is good agreement between the results obtained by the present method and earlier published data. For the numerical calculations, the planes P_1 and P_2 were assumed to be 0.2 cm away from the rectangular ridge. The number of tetrahedra used to discretize the FEM region was 2718. The number of higher order modes considered in the input as well as the output waveguides were 40.

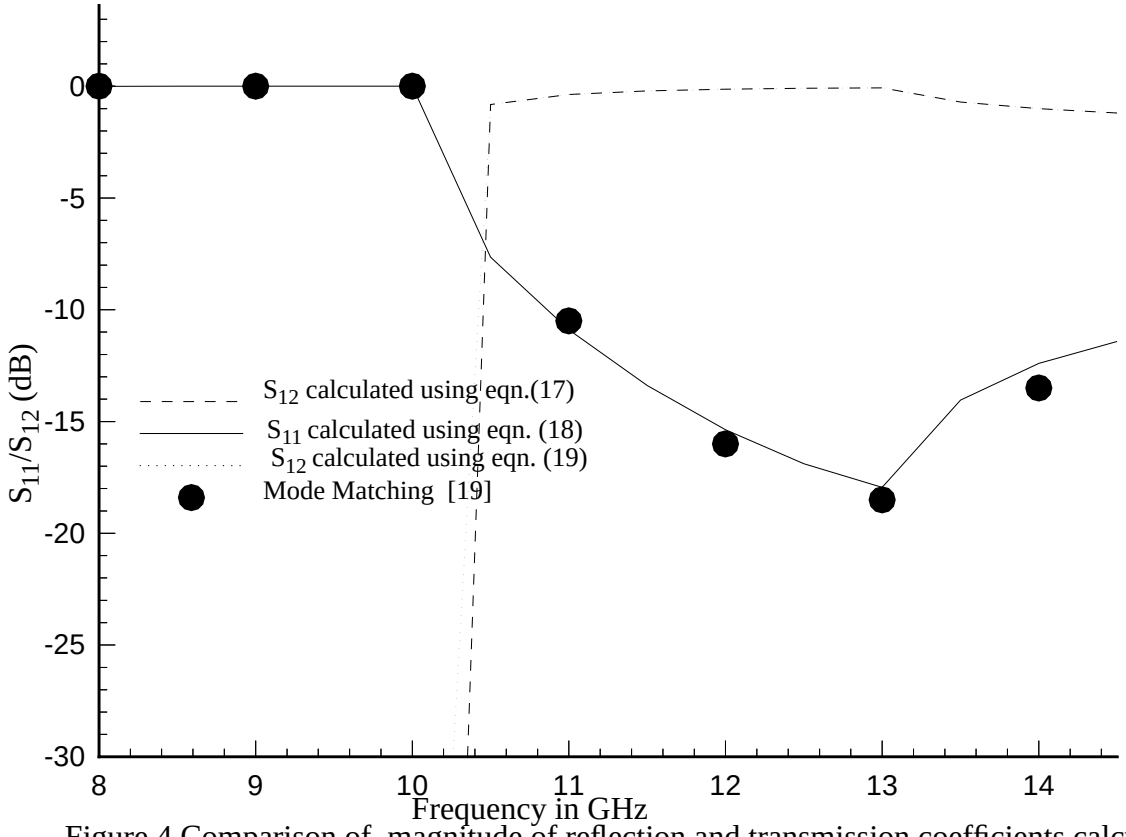

Figure 4 Comparison of magnitude of reflection and transmission coefficients calculat
Finite Element Method and Mode Matching Techniques.

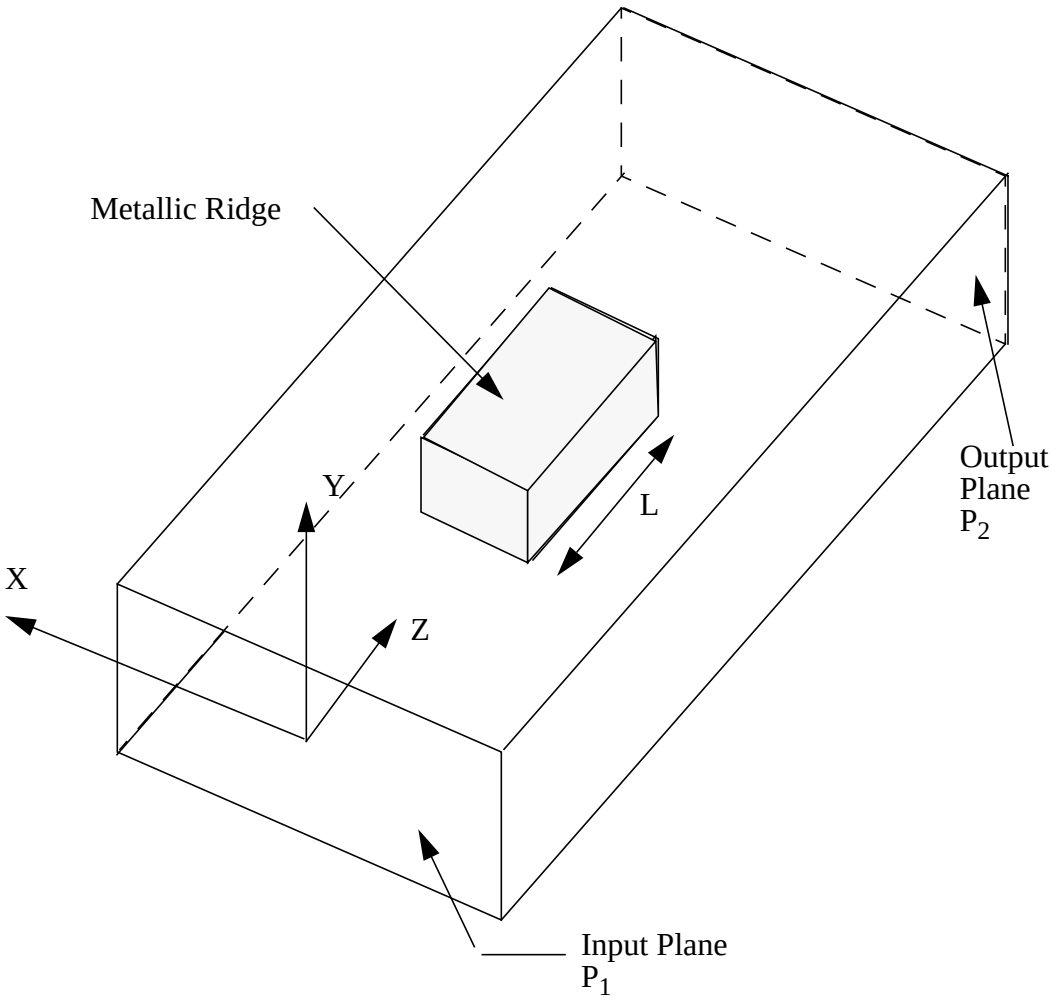

Figure 5(a) Geometry of E-plane ridge discontinuity in a rectangular waveguide .

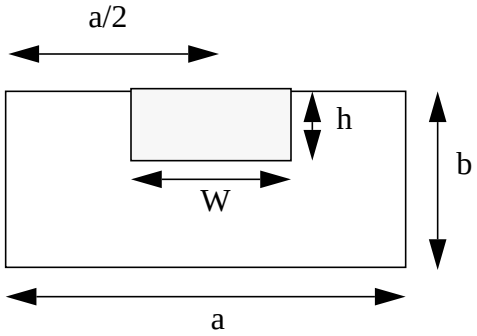

Figure 5 (b) Cross sectional view of E-plane ridge discontinuity in a rectangular waveguide (W= 0.1016cm, h = 0.7619 cm, L = 0.508cm, a = 1.905 cm, b = 0.9524 cm)

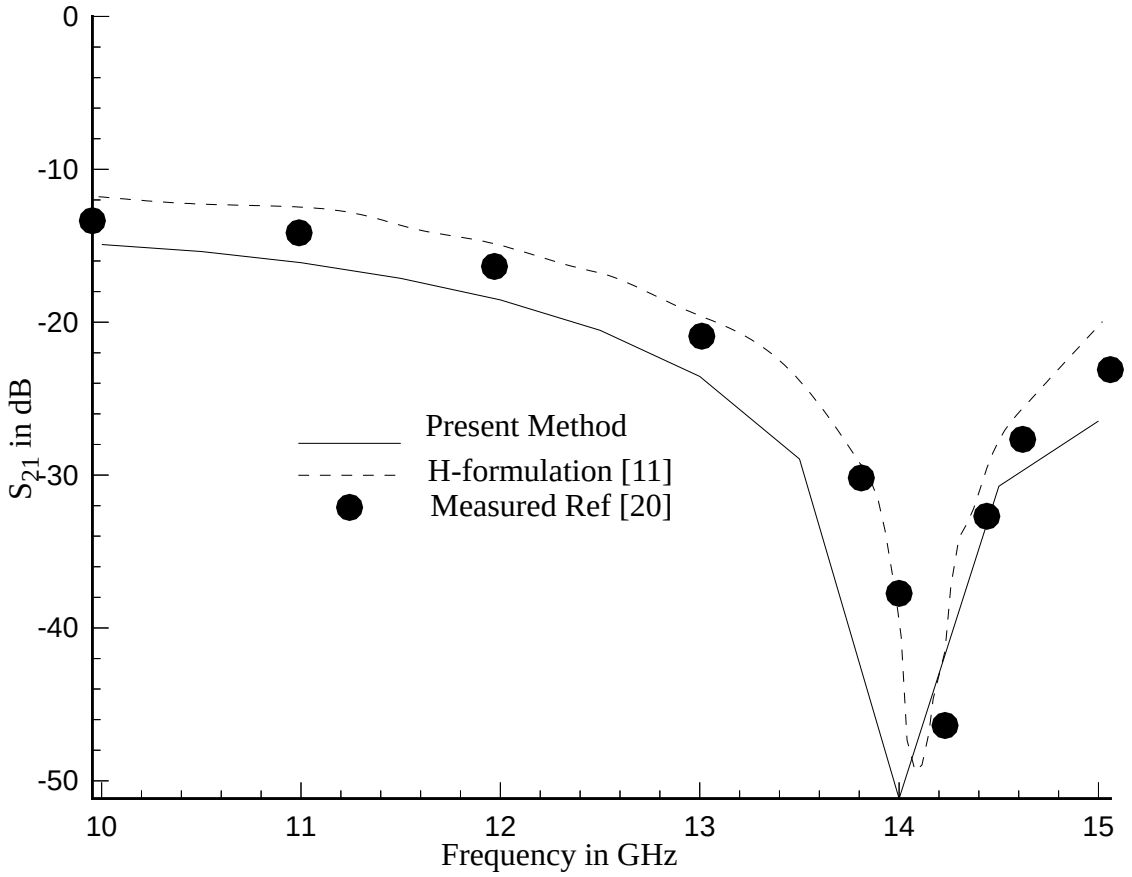

Figure 6 Transmission coefficient of E-plane ridge discontinuity in a rectangular waveguide shown in figure 5.

The third example considered for the validation of the present code is shown in Figure 7. The reference planes P_1 and P_2 were assumed to be 0.5 cm away from the junction. The FEM region was discretized into 2700 tetrahedra and the number of higher order modes considered in each waveguide was 40. The reflection and transmission coefficients calculated using the present code are presented in Figure 8 along with the earlier published data. There is good agreement between the earlier published data and the numerical results obtained using the present code.

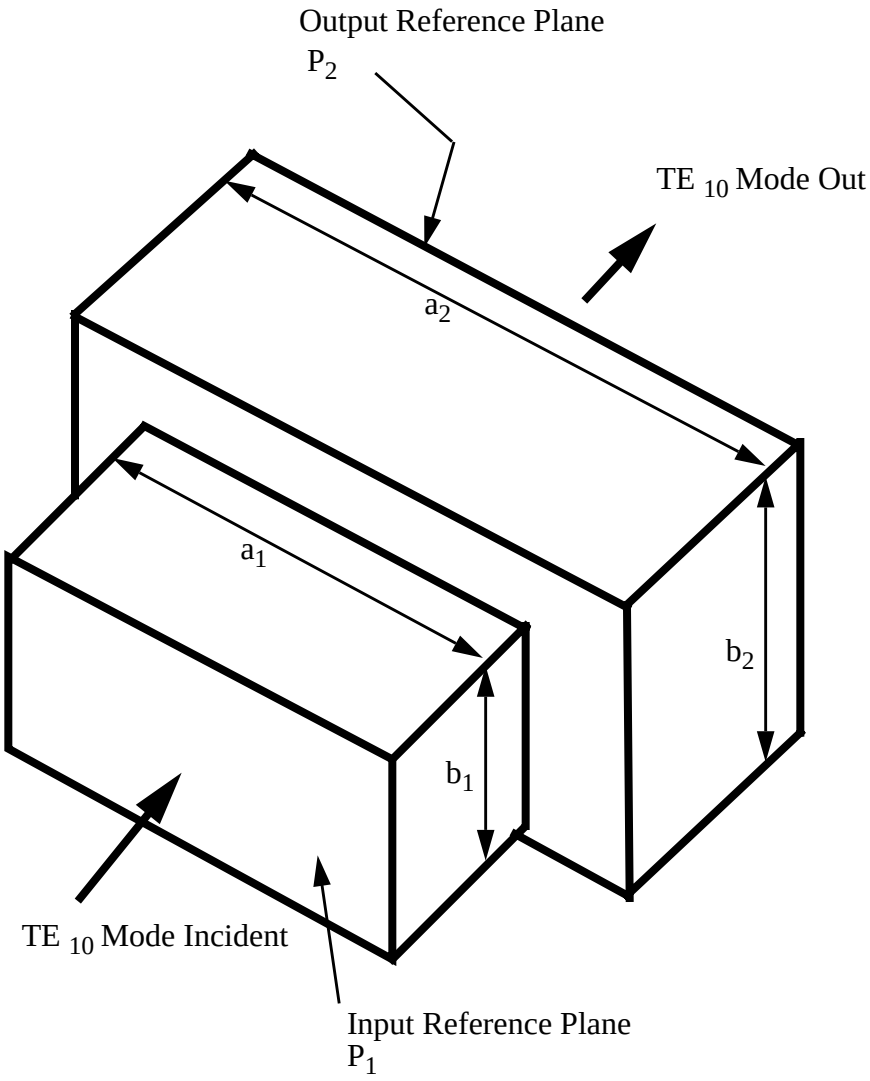

Figure 7 Concentric step discontinuity in a rectangular waveguide; input waveguide dimension (a_1 = 1.58 cm, b_1 = 0.79 cm), output waveguide dimensions (a_2 = 2.29 cm, b_2 = 1.02 cm)

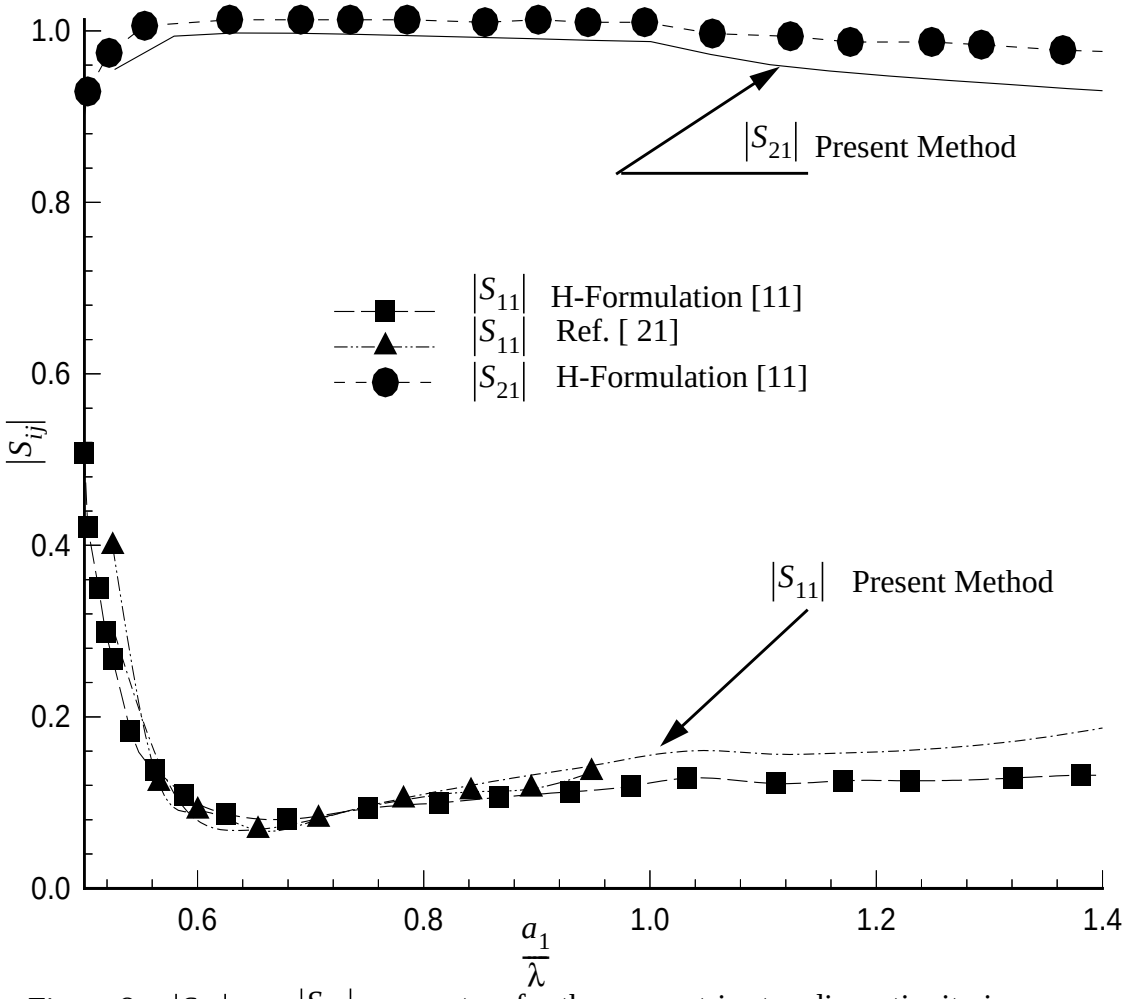

Figure 8 $|S_{11}|$ and $|S_{21}|$ parameters for the concentric step discontinuity in rectangular waveguide shown in figure 7

The discrepency in the results at higher frequencies may be due to the same discretization used for lower and higher frequency range. This causes the results to be less accurate at higher frequencies.

Other discontinuities considered in this report are shown in Figures 9 - 13. The input reflection coefficients calculated using the FEM and MMM as described in the previous section

are presented in Figures 9 -13. Number of higher order modes considered for MMM were 100 modes in input and output waveguides. The number of modes considered (in all of the problems shown here) on the aperture were 20. For FEM the number of elements used were approximately 1200. The numerical results obtained using the FEM and MMM agree well with each other.

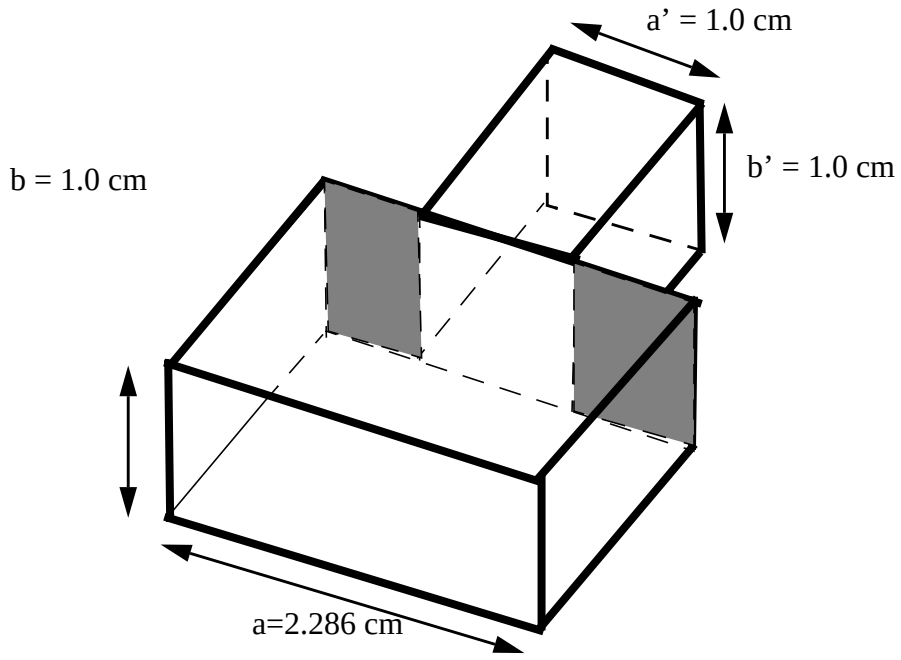

Figure 9(a) Geometry of concentric rectangular waveguide with an inductive junction.

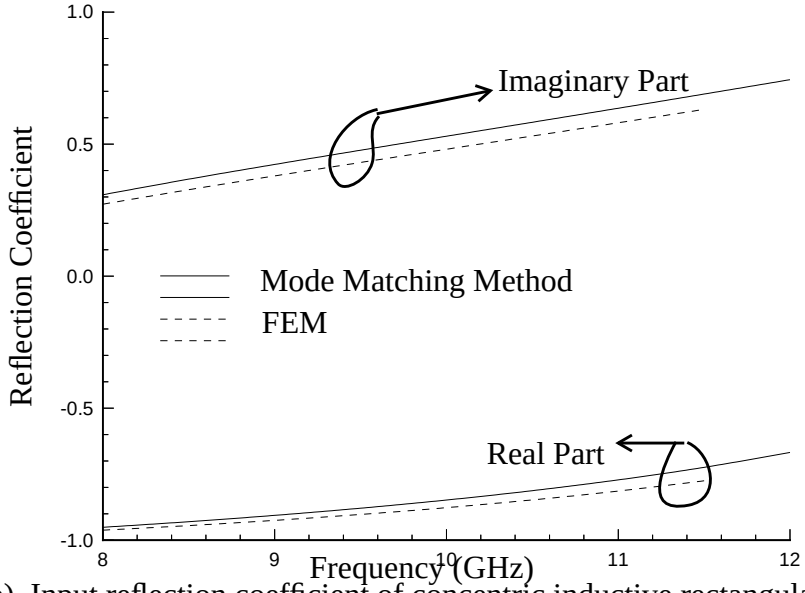

Figure 9(b) Input reflection coefficient of concentric inductive rectangular waveguide junction shown in figure 9(a).

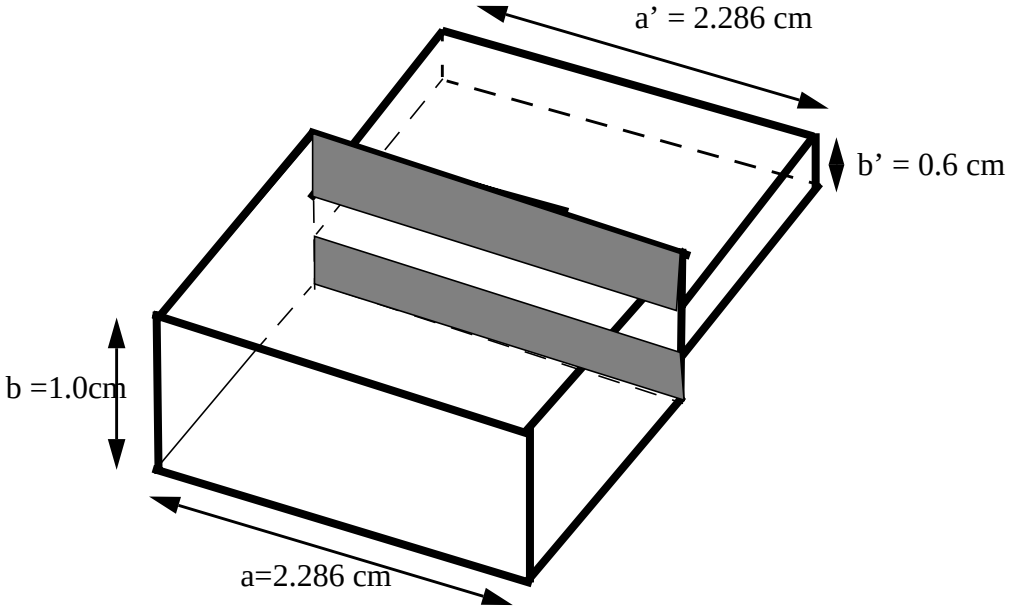

Figure 10(a) Geometry of concentric rectangular waveguide with a capacitive junction.

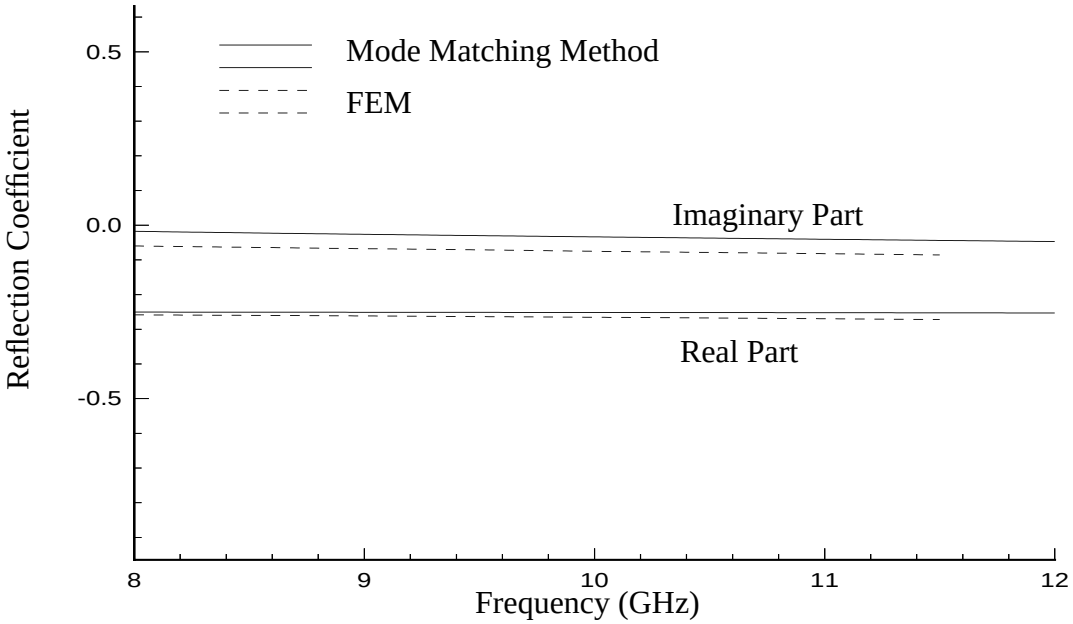

Figure 10(b) Input reflection coefficient of concentric capacitive rectangular waveguide junction shown in figure 10(a).

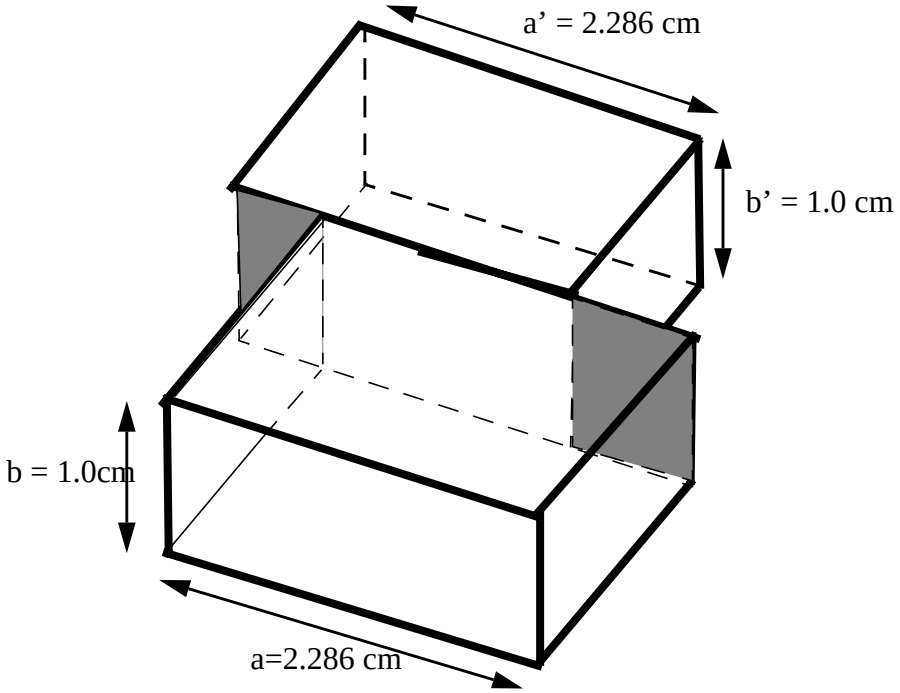

Figure 11(a) Geometry of offset rectangular waveguide inductive junction.

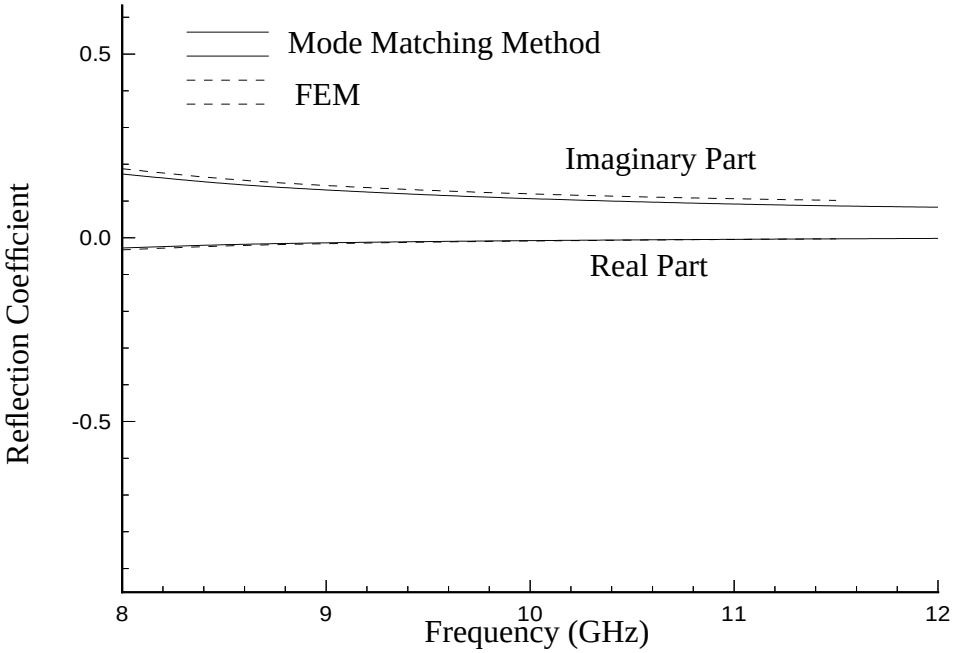

Figure 11(b) Input reflection coefficient of offset inductive rectangular waveguide junction shown in figure 11(a).

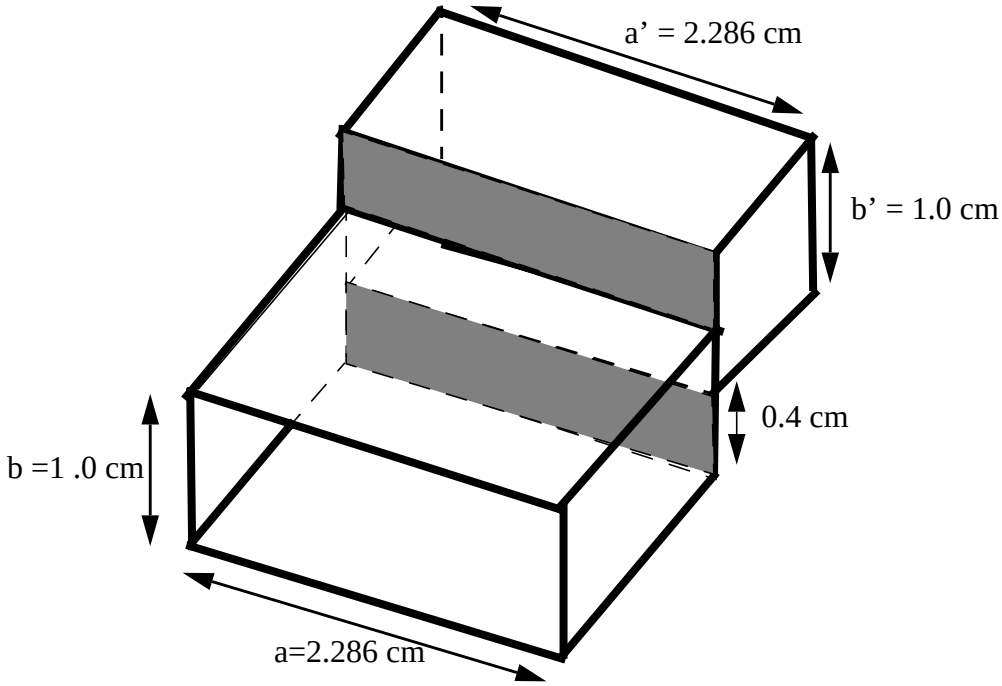

Figure 12(a) Geometry of offset rectangular waveguide capacitive junction.

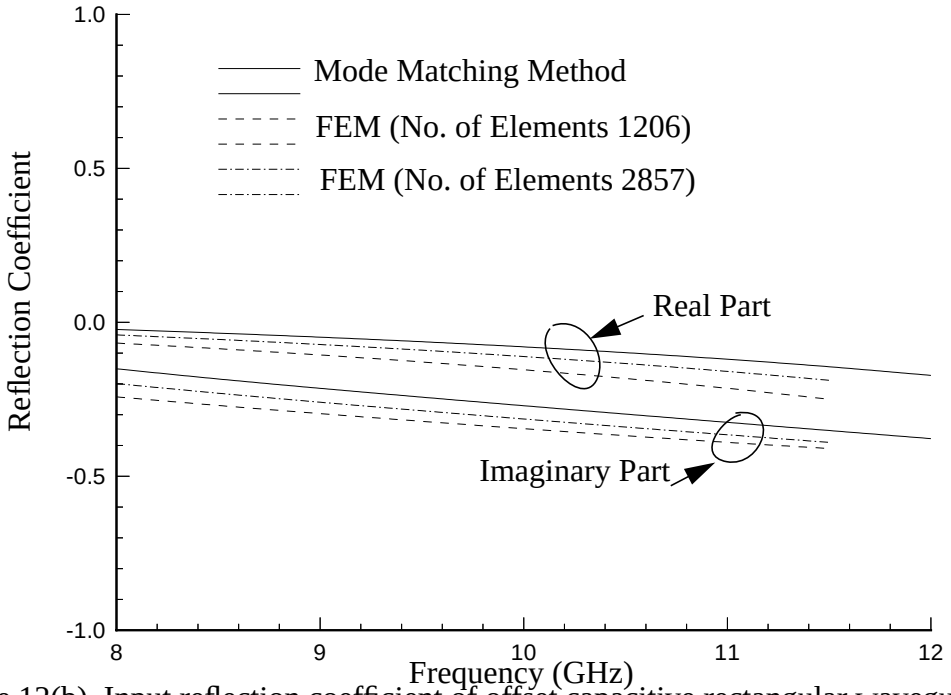

Figure 12(b) Input reflection coefficient of offset capacitive rectangular waveguide junction shown in figure 12(a).

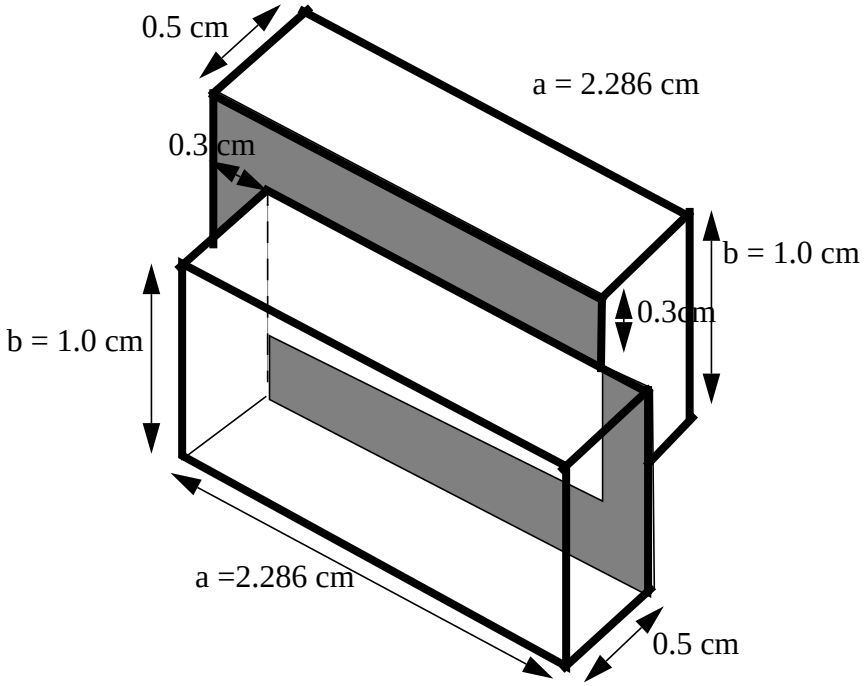

Figure 13(a) Geometry of offset rectangular waveguide junction with x- and y-offset.

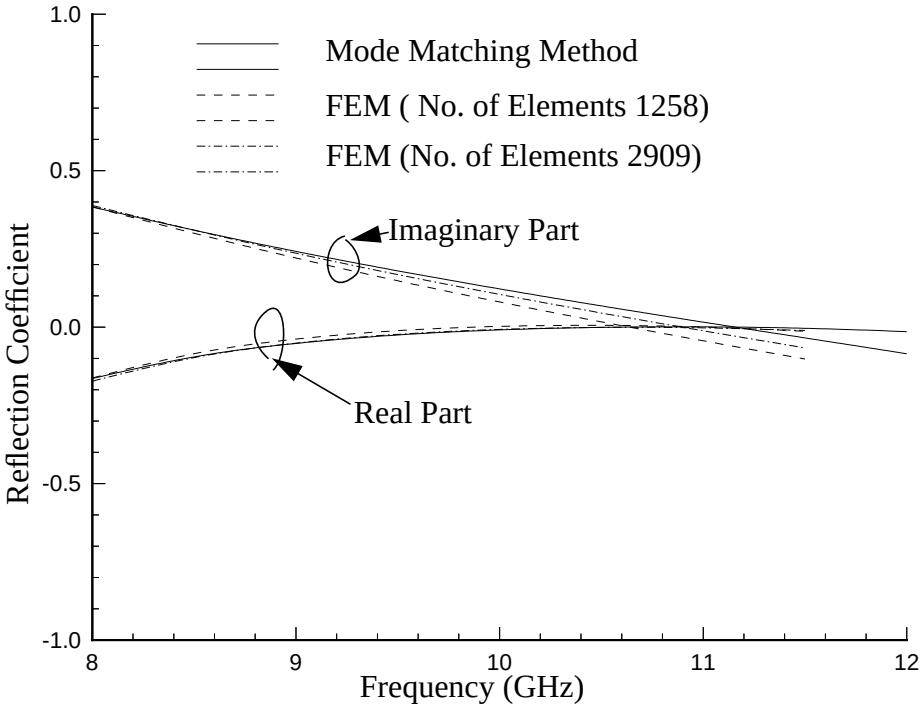

Figure 13(b) Input reflection coefficient of off-set rectangular waveguide junction shown in figure 13(a).

The numerical results shown so far were related to the misalignments in the X-band waveguide. For a S-band waveguide, some typical misalignments analyzed using the FEM and MMM and compared with the measured data taken in the measurement laboratory of ERB are shown in Figures 14-16. The measurements were done using the HP 8510 Network Analyzer. For the FEM analysis the reference planes P_1 and P_2 were selected at 0.5 cm away from the junction. The number of elements used in all cases were around 1258. For the MMM the number of modes consided in both waveguides were 100, and the number of modes used to represent aperture field were 20.

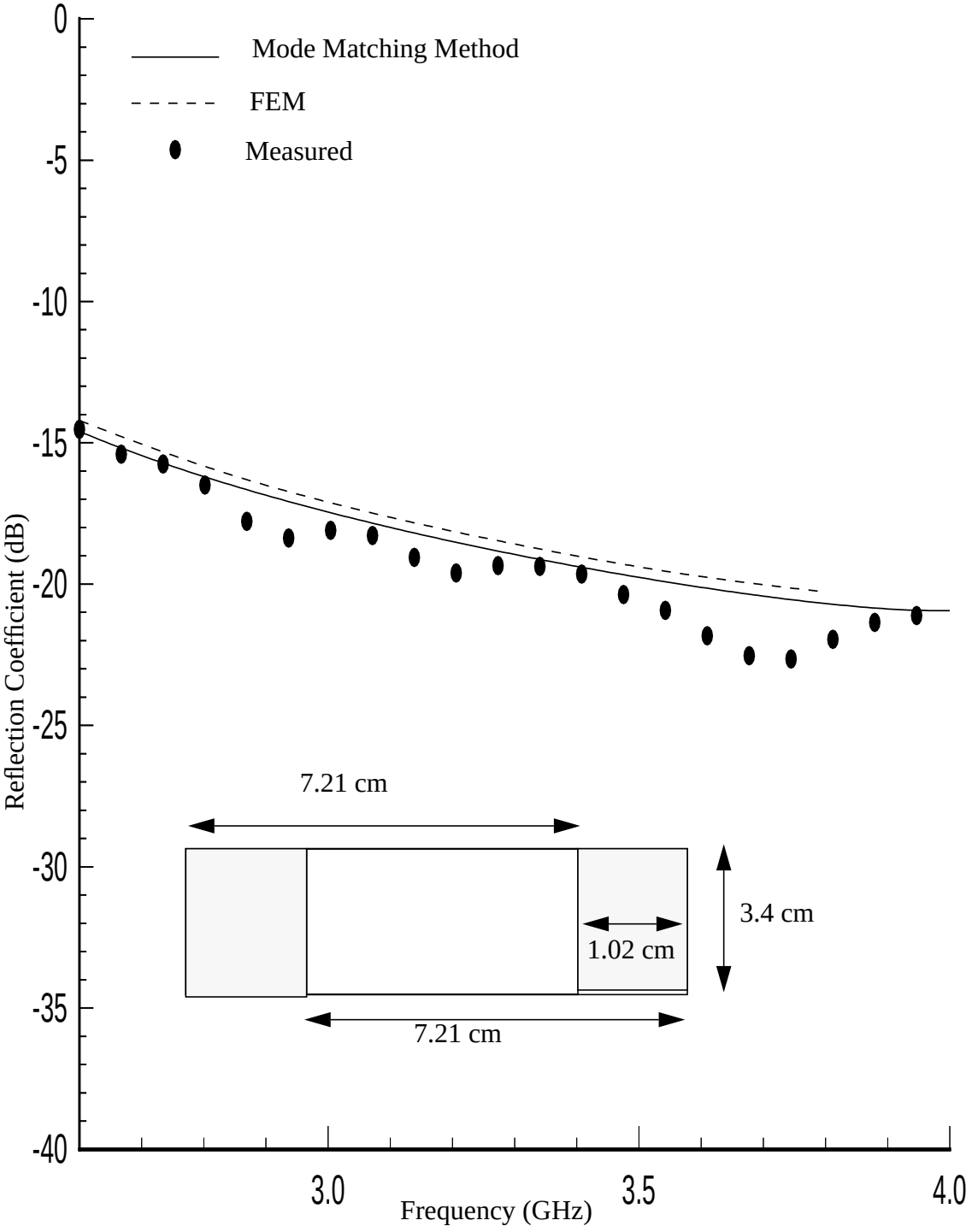

Figure 14 Input reflection coefficient of inductive junction in a S-band rectangular waveguide.

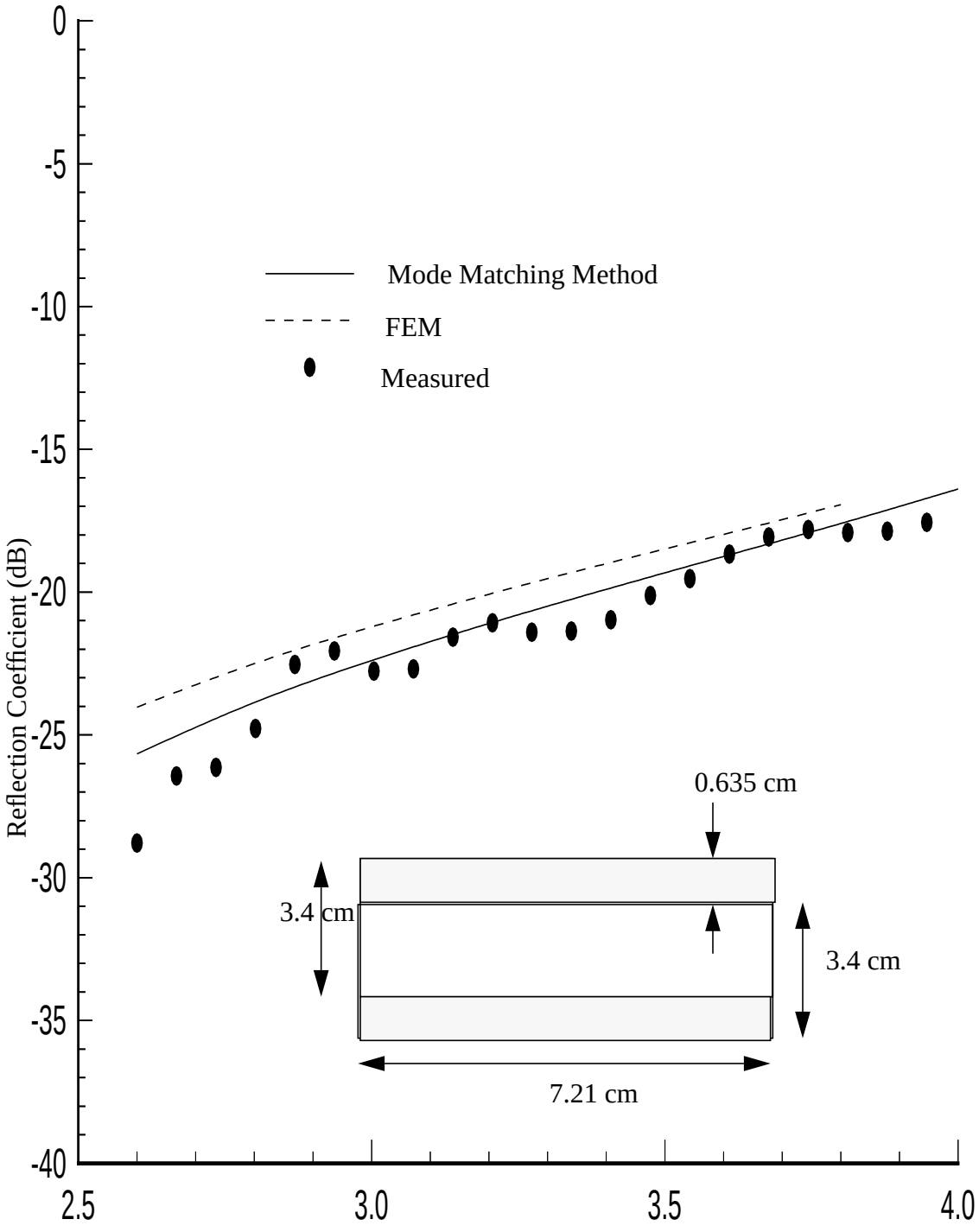
Mode Matching Method
FEM
Measured
Reflection Coefficient (dB)
0
-5
-10
-15
-20
-25
-30
-35
-40
2.5
3.0
3.5
4.0
0.635 cm
3.4 cm
3.4 cm
7.21 cm

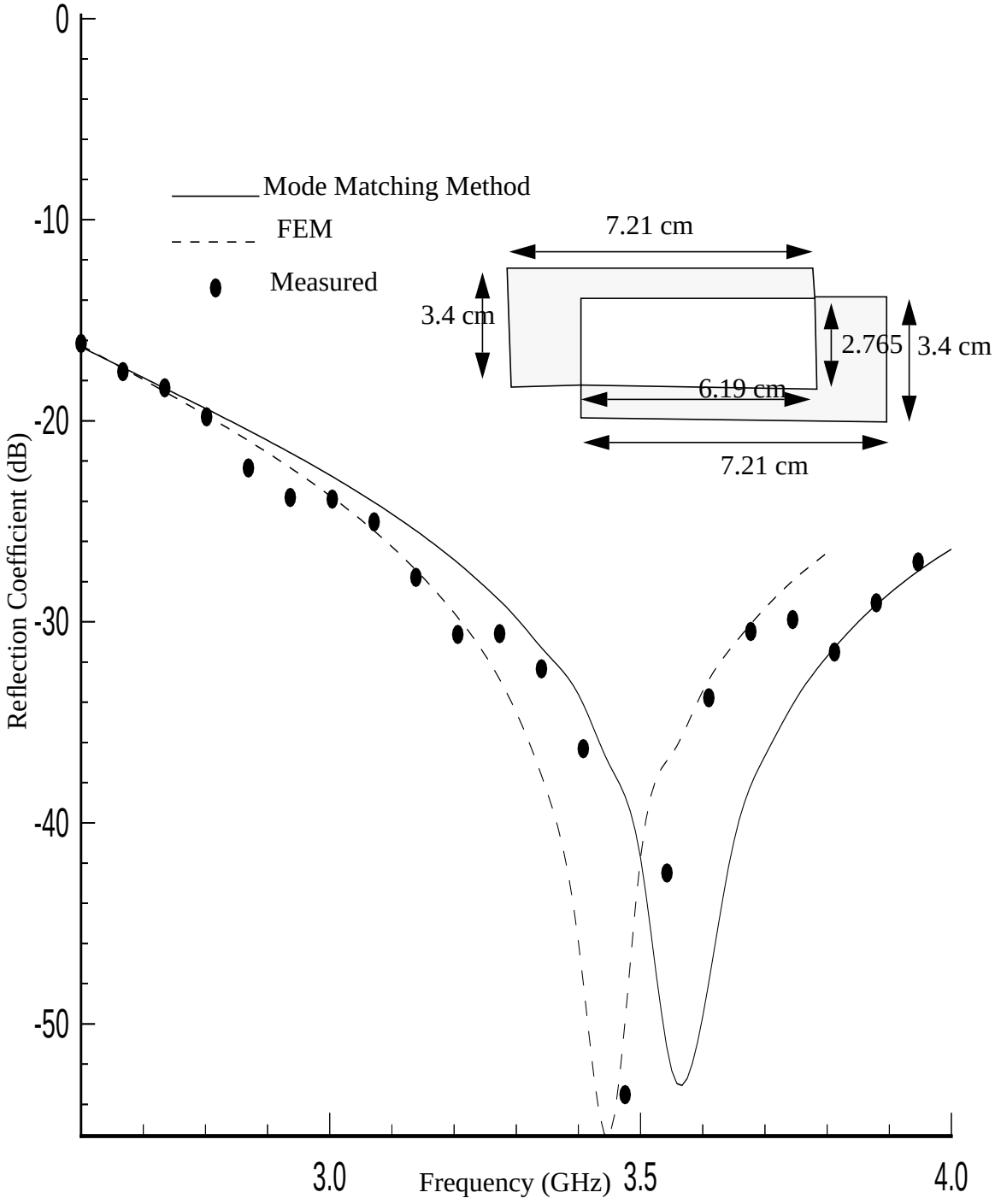

Figure 16 Input reflection coefficient of x- and y-offset junction in a S-band rectangular waveguide.

For application of the FEM to analyze gap between two rectangular waveguide sections we consider S-band rectangular waveguide junction as shown in Figure 17.. The reflection coefficient obtained using the present FEM procedure is presented in figure 17 along with the measured results.

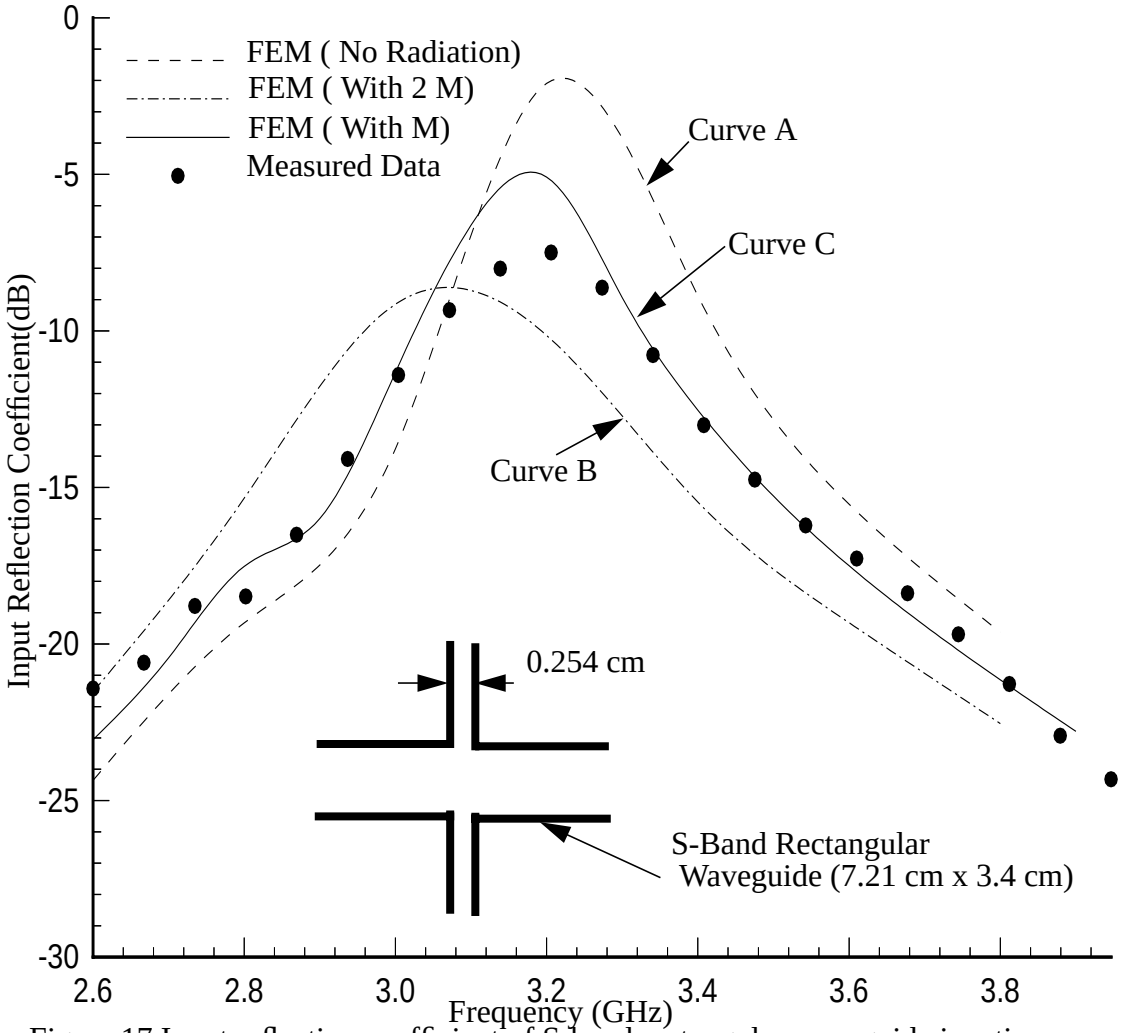

Figure 17 Input reflection coefficient of S-band rectangular waveguide junction with an air gap.

The curve A in Figure 17 shows the input reflection coefficient obtained assuming there is no radiation through the gap aperture. In this simulation the gap opening was not terminated into metal boundary. The curve B in Figure 17 was obtained by assuming the radiating gap aperture is backed by an infinite ground plane. The presence of infinite ground plane is taken into account by considering magnetic current source $\vec{M}$ of amplitude twice that of magnetic current present in the aperture. The curve C in figure 17 shows the input reflection coefficient obtained without an assumption of infinite ground plane. In that case there was no factor two involved in the amplitude of magnetic current source. From the comparison of calculated and measured results in figure 17 it may be concluded that not assuming the presence of infinite ground plane is more appropriate.

4.0 Conclusion

A FEM procedure has been presented to determine complex reflection and transmission coefficients of rectangular waveguide junction discontinuities. The discontinuities that can be analyzed using the present procedure can be E-plane, H-plane, or both. The present procedure can also handle the air gap that may be present between the junctions of two rectangular waveguides. The numerical results obtained from the present method are compared with earlier published results. An excellent agreement between the numerical results obtained by the present code and the earlier published data validates the present method and the code developed.

References

[1] L. Matthaei, L. Young, and E. M. T. Jones, *Microwave Filters Impedance Matching Network, and Coupling Structures*, New York, McGraw-Hill, 1964.

[2] N. Marcuvitz, *Waveguide Handbook, Radiation Laboratory Series,* Vol. 10, New York, McGraw-Hill, 1951.

[3] H. A. Bethe, “Theory of diffraction by small holes, ” Phys. Rev., Vol. 66. pp. 163-182, 1944.

[4] S. B. Cohn, “Electric polarizability of apertures of arbitrary shape, ” Proc. IRE, Vol. 40, pp. 1069-1071, 1952

[5] R. Mittra and W. W. Lee, *Analytical Techniques in the Theory of Guided Waves*, New York, Macmillan, 1971.

[6] T. Itoh, Ed., “*Numerical Techniques for microwave and millimeter wave passive structures,* ” New York, Wiley, 1989

[7] R. R. Mansour and J. Dude, “ Analysis of microstrip T-junction and its applications to the design of transfer switches, ” 1992 IEEE-MTT-S Dig., pp. 889-892.

[8] F. Alessandri, et al, “ Admittance matrix formulation of waveguide discontinuity problems: computer-aided design of branch guide directional couplers, ” IEEE Trans. Microwave Theory and Techniques, Vol. 36, No. 2, pp 394-403, Feb. 1988.

[9] M. Guglielmi and C. Newport, “ Rigorous, multimode equivalent network represntation of inductive discontinuities, ” IEEE Trans. Microwave Theory and Techniques, Vol. 38, No. 11, pp 1651-1659, Nov. 1990.

[10] A. A. Melcon, et al, “New simple procedure for the computation of the multimode admittance or impedance matrix of planar waveguide junctions,” IEEE Trans. Microwave Theory and Techniques, Vol. 44, No. 3, pp 413-416, March 1996

[11] K. Ise, et. al, “Three-dimensional finite element method with edge elements for electro-magnetic waveguide discontinuities, ” IEEE Trans. Microwave Theory and Techniques, Vol. 39, No. 8, pp. 1289-1296, August 1991.

[12] J. F. Lee, et. al, “ Full wave analysis of dielectric waveguides using tangential vector finite elements, ” IEEE Trans. Microwave Theory and Techniques, Vol. 39, No. 8, pp.1262-1271, August 1991.

[13] L. Zhou and L. E. Davis, “Finite element method with edge elements for waveguides loaded with ferrite magnetized in arbitrary direction, ” IEEE Trans. Microwave Theory and Techniques, Vol. 44, No. 6, pp. 809-815, June 1996.

[14] L. T. Tang, M. S. Nakhla and R. Griffith, “Analysis of lossy multiconductor transmission lines using the asymptotic waveform evaluation technique, ” IEEE Trans. Microwave Theory and Techniques, Vol. 39, pp. 2107-2116, December 1991.

[15] L. T. Pillage and R. A. Rohrer, “Asymptotic waveform evaluation for timing analysis, ” IEEE Computer Aided Design, pp. 352-366, 1990.

[16] R. F. Harrington, *Time-harmonic electromanetic fields*, McGraw-Hill Book Company, New York,1961.

[17] J. Jin, *The finite element method in electromagnetics*, John Wiley & Sons, Inc., New York, 1993.

[18] R. E. Collins, *Foundation for microwave engineering*, *Chapter 4*, McGraw-Hill Book Company, New York, 1966.

[19] A. Weisshaar, M. Mongiardo, and V. K. Tripathi, “CAD-oriented equivalent circuit modelling of step discontinities in rectangular waveguides, ” IEEE Microwave and Guided Wave Letters, Vol. 6, No. 4, pp. 171-173, April 1996.

[20] R. Mansour, et al., “Simplified description of the field distribution in finlines and ridge waveguides and its application to the analysis of E-plane discontinuities, ” IEEE Trans. Microwave Theory and Techniques, Vol. MTT-36, pp. 1825-1832, Dec. 1988.

[21] H. Patzelt and F. Arndt, “Double-plane steps in rectangular waveguides and their application for transformers, irises and filters, ” IEEE Trans. Microwave Theory and Techniques, Vol. MTT-30, pp. 771-776, May 1982.